Hindawi
Advances in Materials Science and Engineering
Volume 2020, Article ID 4761854, 8 pages
https://doi.org/10.1155/2020/4761854

Research Article

Electrochemical Performance of Steel Embedded in CSA Concrete and Its Interfacial Microstructure

Meimei Song,[1,2] **Qiu Li**,[2] **Ke Wu**,[3] **and Yihua Dou**[1]

[1]*School of Mechanical Engineering, Xi'an Shiyou University, Xi'an 710065, China*
[2]*State Key Laboratories of Silicate Materials for Architectures, Wuhan University of Technology, Wuhan 430070, China*
[3]*School of Mechanical and Materials Engineering, University College Dublin, Dublin, Ireland*

Correspondence should be addressed to Qiu Li; qiu-li@whut.edu.cn and Yihua Dou; yhdou@vip.sina.com

Received 16 March 2020; Revised 22 May 2020; Accepted 3 June 2020; Published 6 July 2020

Academic Editor: Marián Palcut

Calcium sulfoaluminate cement (CSA) is a low-carbon cementitious material that significantly reduces alkalinity and produces calcium hydroxide-free (CH-free) matrix environment in comparison to ordinary Portland cement (OPC). It might be, however, less efficient towards the passivation of steel in concrete and further investigation before widespread adoption is required. In this project, scanning electron microscopy/energy dispersive X-ray spectroscopy (SEM/EDX) on polished samples was employed to provide the interfacial characterization of steel reinforced CSA concrete and study the relationship of interfacial quality and corrosion resistance of the embedded steel. The galvanostatic polarization behavior indicates that the steel embedded in CSA concrete remains passive for 28 days in absence of Cl^- ions and carbonation. Microstructure analysis has shown that there is an Al-enriched layer at interfacial zone in CSA concrete with the main hydration product of AH_3, which is also alkaline and is expected to improve the steel passivity. Furthermore, the interfacial zone has markedly reduced porosity compared to the bulk matrix, which leads to reduced possibility of current flow between anode and cathode and therefore improves the corrosion resistance of the embedded reinforcement.

1. Introduction

Steel reinforced concrete has become the most important construction material in engineering in present days; however, the cement industry is challenged as it significantly contributes to global CO_2 emissions every year. Therefore, a low-carbon alternative to ordinary Portland cement (OPC) is of great importance for environmental benefits. Due to the requirement of less amounts of limestone in the raw material and reduced burning temperature, calcium sulfoaluminate (CSA) cement has been developed as a low-carbon cementitious material [1, 2]. The use of CSA cement has the potential of reducing up to 35% of CO_2 emissions from the cement industry [3]. It also has high early strength, reduced drying shrinkage and improved anti-freeze property.

Maintaining high pH at the steel/concrete interfacial zone (ITZ) is essential to guarantee the normal engineering function of the embedded rebar in concrete over structural lifetimes. However, a pore solution with lower pH value, at around 11, has been developed within CSA cement [4]. Debates still continue on the passivation of the embedded steels in CSA concrete matrix, which limits a wider application of CSA cement [5–7]. Research by Kalogridis et al. [5] demonstrated that reduced alkalinity in CSA cement pore solution may have an adverse effect on the corrosion resistance of embedded reinforcement and is likely to increase the corrosion risk. Research by Glasser and Zhang [6] revealed an excellent protection of embedded mild steel by CSA cement matrix after 14 years of service. Carsana et al. [7] stated that the pore solution of CSA cement was enough alkaline to passivate the embedded reinforcement, showing a high electrical resistivity of 100 Ω·m at 1 d.

For microstructural reasons, the nature of steel/concrete ITZ is a key factor in governing the corrosion resistance of the embedded reinforcement. Numerous studies have been carried out to investigate the relationship between the

quality of steel/concrete ITZ and the corrosion resistance of the embedded reinforcements in steel reinforced OPC concrete, on both macroscopic and microscopic levels [8–12]. It was reported that the steel/concrete ITZ with superior quality may reduce the time to corrosion initiation or slow down the corrosion rate [13]. Increased volumes of air voids in the vicinity of steel may either initiate or accelerate the corrosion by facilitating a rapid oxygen uptake, thereby promoting the cathodic oxygen reduction reaction [8].

Therefore, it is essential to investigate the microstructural characteristics and chemical compositions at steel/concrete ITZ in steel reinforced CSA concrete, before more green and durable steel reinforced concretes can be produced. The present research mainly focuses on the chemical compatibility between the hydrated CSA cement and steel reinforcement. Electrochemical performance of steel reinforcement and microstructural characteristics at steel/concrete ITZ are examined in this study.

2. Materials and Methods

A commercial CSA cement was used in this research. Steel bars with a diameter of 10 mm were used as the reinforcements, and they were gently wiped with acetone to remove a loose rust layer on the surface. Standard steel reinforced CSA concrete cubes were then cast with four steel bars inserted vertically into the concrete. For comparison, steel reinforced concretes made by OPC cement were also cast as references. Mixing designs of both CSA and OPC concrete are presented in Table 1.

In order to investigate the hydration mechanism of CSA cement, a pure CSA cement paste with a w/c ratio of 0.69 was prepared for X-ray diffraction (XRD) and thermal analyses. Samples were cured at 21°C under water in a sealed plastic bag for 1 d, 7 d and 28 d. Pure Portland cement paste (CEM 0049 32.5R provided by Hanson Cement) with a w/c ratio of 0.69 was also produced according to EN 197-1 [14] as a reference sample. Chemical compositions of the two cement systems are listed in Table 2. Clinker compositions of the CSA cement are Ye'elimite 62.3%, belite 22.5%, and gypsum 15.2%.

Thermal analysis was undertaken by Stanton Redcroft Simultaneous Thermal Analysis STA-780. At specified curing ages, a cement paste hydration was stopped by immersion in acetone [15] and freshly ground cement powder was heated in a furnace under constant flow of nitrogen at ramping rate of 20°C/min. For the analysis of crystalline hydration products, XRD was studied by Bruker D8, operating at 40 kV and 40 mA between 5° and 80° (2θ) at a step size of 0.0333 degree.

In order to examine the passivation of reinforcement embedded in CSA concrete, polarization behavior was investigated in a standard three-electrode cell controlled by potentiostat (Autolab PGSTAT 302N potentiostat from Ecochemie, The Netherlands). After curing at 21°C for 28 d, the steel bars were positioned as working electrodes, stainless steel ruler was used as a counter electrode, and copper-copper sulfate electrode was the reference electrode. A constant 50 μA/cm^2 current was applied through a saturated calcium hydroxide (CH) solution.

In this project, scanning electron microscopy analysis (SEM) was undertaken by JEOL JSM-5800LV, and back-scattered electron (BSE) mode was chosen to investigate the microstructural characteristics at steel/concrete ITZ. Meanwhile, spot analysis for representative points at ITZ was carried out by Energy dispersive X-ray (EDXA) detector. Digital image analysis technique performed on KS 300 imaging system (developed by Carl Zeiss Vision) was used to study the porosity at ITZ. Detailed procedures of imaging analysis technique can be found in the previous work [16].

3. Results and Discussion

3.1. STA. Differential thermal analysis (DTA) curves of hydrated CSA cement paste cured for 1 d, 7 d, and 28 d are given in Figure 1(a). In the 1 d aged sample, a significant endothermic peak at 135°C indicates the formation of ettringite [17]. Ettringite results from the rapid reaction of calcium sulfoaluminate with water, while gypsum is available (equation (1)). In the 7 d aged samples, ettringite formation can also be traced at 135°C. Besides this, there is another broad endothermic peak at about 160°C, which can be related to the dehydration of strätlingite [17]. Formation of strätlingite will be further discussed in Section 3.2. The adjacent small step at 180–220°C is linked to the occurrence of monosulfate [17], which results from the hydration of calcium sulfoaluminate with the depletion of gypsum (equation (2)). Water loss of AH_3 is also found in hydrated CSA cement at all the three investigated curing ages, relating to a small endothermic peak at 280–300°C [18]. It is generated from the hydration of calcium sulfoaluminate both with and without the occurrence of gypsum as shown in equations (1) and (2). At 28 d, two heat endotherms at 125–180°C become considerably broader with indefinite boundaries, which can normally be attributed to ettringite and strätlingite. The strongest peak has a tendency to shift towards higher temperatures, suggesting a relative predominance of strätlingite over ettringite at 28 d.

$$C_4A_3\overline{S} + 2C\overline{S}H_2 + 34H \longrightarrow C_3A \cdot 3C\overline{S} \cdot 32H + 2AH_3 \text{ (ettringite formation)} \quad (1)$$

$$C_4A_3\overline{S} + 18H \longrightarrow C_3A \cdot C\overline{S} \cdot 12H + 2AH_3 \text{ (monosulfate formation)} \quad (2)$$

DTA curves for hydrated OPC paste cured for 1 d, 7 d, and 28 d are shown in Figure 1(b). It is obvious that the DTA curves consist of a strong central peak at about 120°C, which is indicative of the presence of calcium silicate hydrate (C-S-H) gel, with two neighboring broad endotherms at both sides, which can be related to the evaporation of weakly bound pore water at 100°C and dehydration of ettringite at about 180°C. With ageing, the strong central endotherm tends to become broader and deeper, suggesting an

Table 1: Mixing designs of CSA and OPC concrete.

	Cement (kg/m^3)	Water (kg/m^3)	Water/cement (w/c) ratio	Fine aggregate (kg/m^3)	Coarse aggregate (kg/m^3)	Super plasticiser (%)
CSA	309	213	0.69	740	1100	1.0
OPC	309	213	0.69	740	1100	1.0

Table 2: Oxide composition of the CSA and OPC cement powder (by wt. %).

	CaO	SiO_2	Al_2O_3	SO_3	Fe_2O_3	MgO	K_2O	Na_2O	TiO_2	SrO	BaO	Mn_3O_4	LOI
CSA	42.33	9.00	33.82	8.83	1.35	2.29	0.22	0.12	1.61	0.07	0.02	0.03	0.31
OPC	62.14	19.42	4.83	4.81	1.95	2.13	0.75	0.24	0.24	0.07	0.02	0.07	3.33

LOI: loss on ignition.

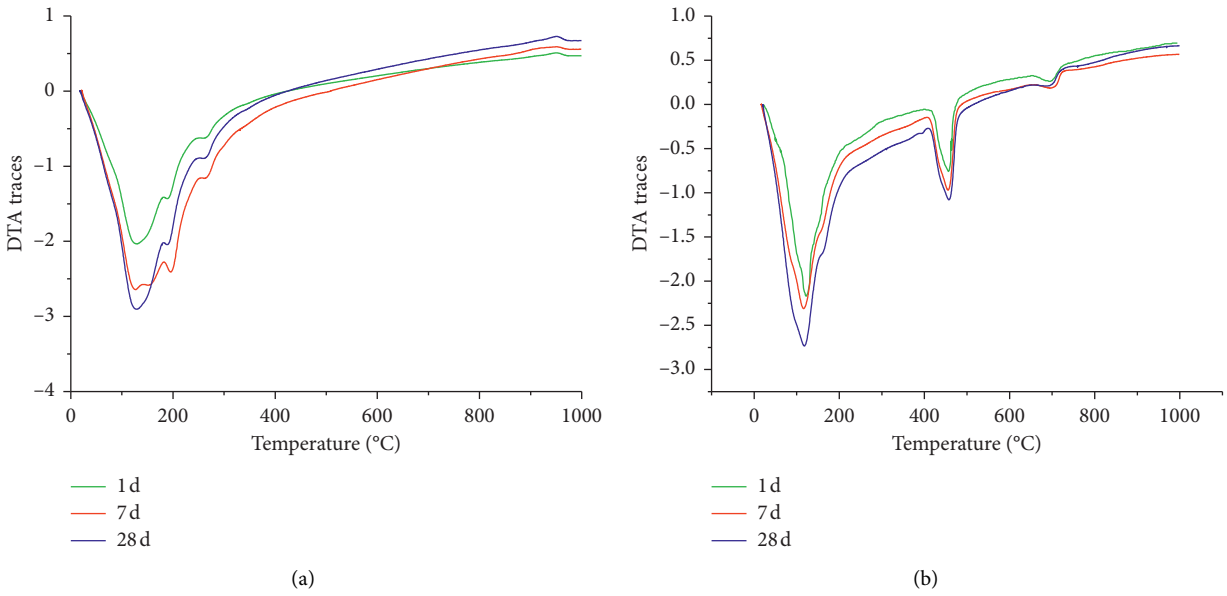

Figure 1: STA results of hydrated (a) CSA cement paste and (b) OPC paste cured at 21°C for 1 d, 7 d, and 28 d.

increased C-S-H gel formation. A prominent shoulder at ~200°C is representative of the formation of monosulfate [17], and this peak becomes broader with increasing curing age. The subsequent step at about 420°C is indicative of the formation of CH [19], which is one of the main hydration products of OPC paste. In addition, a small peak at about 700°C indicates the existence of calcite [19], which is mainly caused by incidental carbonation of CH.

3.2. X-Ray Diffraction. XRD results of CSA cement powder and hydrated CSA cement pastes cured at 1 d, 7 d, and 28 d are shown in Figure 2. Ye'elimite can be traced in CSA cement powder as the main clinker phase. It reacts with water and is consumed during 28 d. Remnants of belite at 28 d demonstrate its lower reactivity and relatively slower hydration process compared to Ye'elimite. Moreover, absence of CH can be observed in the hydrated CSA paste at all the investigated samples. Crystalline hydration product is mainly ettringite at early ages. With the progress of

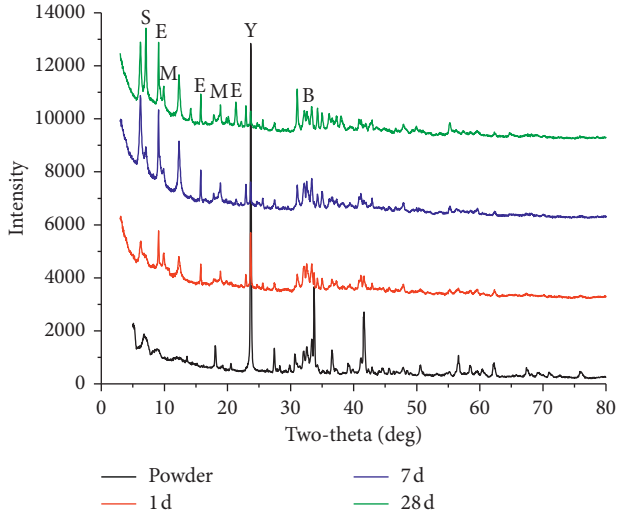

Figure 2: XRD pattern of CSA cement powder and hydrated CSA cement pastes cured at 21°C for 1 d, 7 d, and 28 d. S, strätlingite; E, ettringite; M, monosulfate; Y, Ye'elimite; B, belite.

hydration, increasing amounts of strätlingite and monosulfate (both AFm phases but with different interlayer anions) are formed and gradually dominate in the aged sample, which agrees with the DTA results in Figure 1(a). Strätlingite is generated by the continuous consumption of belite and AH_3 gel:

$$C_2S + AH_3 + 5H \longrightarrow C_2ASH_8 \,(\text{strätlingite formation}) \quad (3)$$

3.3. Electrochemical Tests. Polarization potential-time curves of steel reinforced CSA and OPC concrete are presented in Figure 3. The polarization potential rapidly increases to a value of about 600 mV at 2 min. As duration of polarization increases, the potential slightly decreases from 608 mV to 553 mV. Subsequently, a steady value is maintained at about 550 mV. Therefore, it can be concluded that the reinforcement embedded in CSA concrete is passive and can protect the steel from corrosion at this stage. Similar conclusions can be obtained for the reference OPC sample.

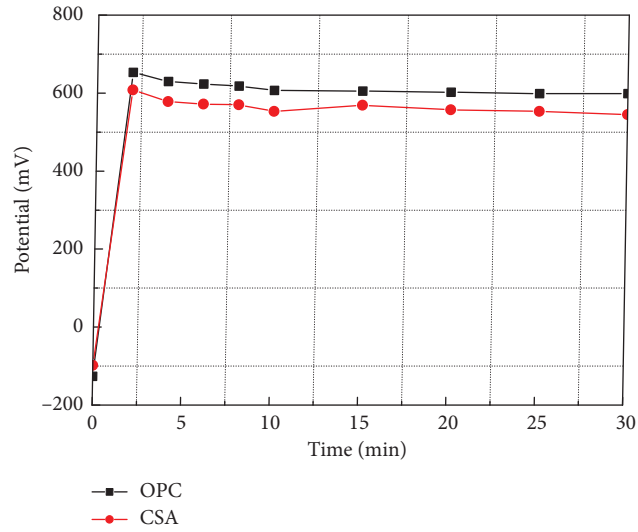

Figure 3: Polarization potential-time curves of steel reinforced CSA and OPC concrete.

3.4. SEM

3.4.1. ITZ in Steel Reinforced CSA Concrete. To find out the potential correlation between steel/concrete ITZ and passivation of the embedded steel, microstructure of steel reinforced CSA concrete aged for 28 d is characterized in Figure 4. Individual phases in the BSE image include the steel reinforcement, unhydrated cement clinker, and ettringite. Steel reinforcement has the lightest color and is surrounded by a continuous rust layer. Accordingly, unhydrated cement clinker displays the lightest grey scale within the matrix. Block-shaped ettringite with lengths of about 10 μm can be found in the bulk matrix. The particles are connected to each other, forming interlocking networks with significant internal porosity. Large voids are also presented in the matrix.

A close contact between CSA concrete and reinforcement is observed, and fewer air voids exist at ITZ than those in the bulk matrix. The porosity at ITZ has been quantified by digital imaging analysis technique, as shown in Figure 4(b). It is obvious that there is a significantly reduced porosity at ITZ (within the first 25 μm) than that in the bulk matrix; this is because of the availability of abundant water at ITZ due to the hydrophobicity of steel. Excessive water could facilitate a higher hydration degree, which results in a refined and densified microstructure with reduced porosity. The average porosity in bulk matrix is as high as 6.5%, and this can be attributed to the interlocking structures of ettringite with great porosity. However, these porous networks are clustered independently in the matrix, with transportation of detrimental ions restricted to some extent. Moreover, owning to the refined porosity at ITZ, these detrimental ions are difficult to penetrate into the reinforcement surface. Therefore, a current flow between anode and cathode mediated by pore solution could be restricted by reduced porosity at ITZ, and thus the electrochemical reaction is less likely to occur.

According to the EDX mapping, Al-rich areas with varying widths can be observed on the steel surface. Meanwhile, a very thin sulfur layer is also clustered on the rebar surface, which may be assigned to either ettringite or monosulfate if combined with the mapping of Al (and, to less extent, Ca). EDX spot analysis for typical Point '1' at ITZ suggests that corresponding Al/Ca atomic ratio is as high as 2.36, compared to a value of 0.33 for pure ettringite and 0.5 for pure AFm. The Al-enriched hydrating phases with different thicknesses on steel surface are presumably considered to be fine intermixtures of AH_3 gel and other Ca-included hydration phases such as ettringite and monosulfate, according to the Ca signal in Figure 4(c). Similar to the high alkaline CH layer at ITZ in steel reinforced OPC concrete, there is an Al-enriched layer at ITZ in CSA concrete with the main hydration product of AH_3, which is alkaline and is therefore expected to improve the steel passivity [7].

Therefore, the Al-enriched phases at ITZ are expected to passivate the steel by reducing porosity and maintaining alkalinity by AH_3 formation.

3.4.2. ITZ in Steel Reinforced OPC Concrete. Microstructure of steel reinforced OPC concrete aged for 28 d is illustrated in Figure 5. As the reference OPC sample has a high w/c ratio of 0.69, a higher degree of hydration has been achieved, and anhydrous cement clinker is seldom observed in the bulk matrix. There is an overall close contact between the concrete matrix and the embedded reinforcement; however, microstructural defects of clustered air voids can be observed occasionally at ITZ. Porosity data at ITZ in Figure 5(b) suggests that SEM-resolvable porosity near the steel surface (~5 μm distance away from steel surface) is as high as ~5.5% compared to an average 1% in the bulk matrix. Increased levels of porosity near the steel surface (within 5 μm) may provide an increased frequency of ion transport in the vicinity of reinforcement, particularly for detrimental Cl^- and O^{2-}, which consequently may lead to higher possibility of reinforcement corrosion initiation. This is in

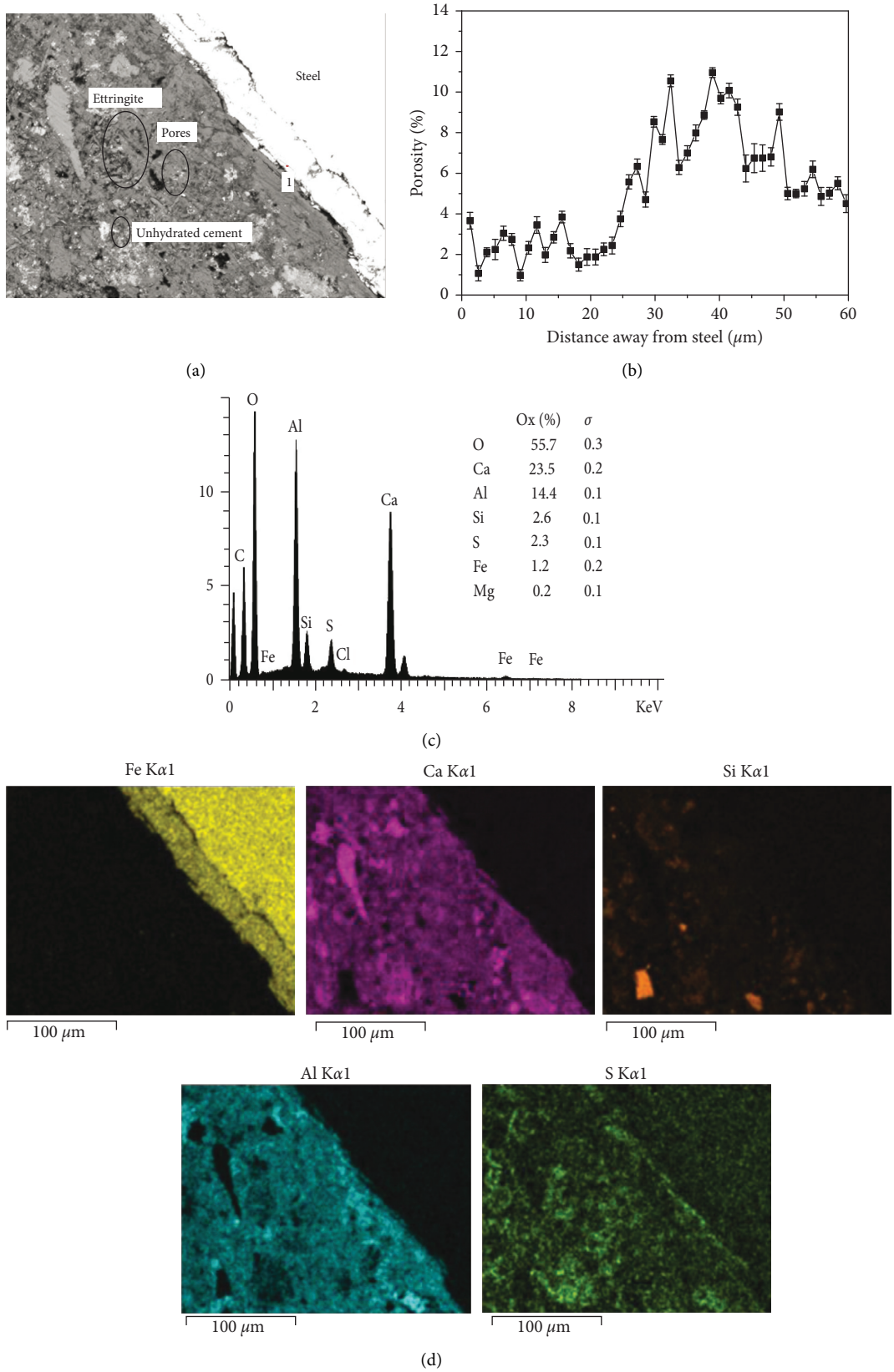

Figure 4: Microstructure of steel reinforced CSA concrete aged for 28 d: (a) microstructure of steel reinforced CSA concrete, (b) porosity at ITZ, (c) EDXA spot analysis of Point '1' at ITZ, and (d) elemental mappings of Fe, Ca, Si, Al, and S.

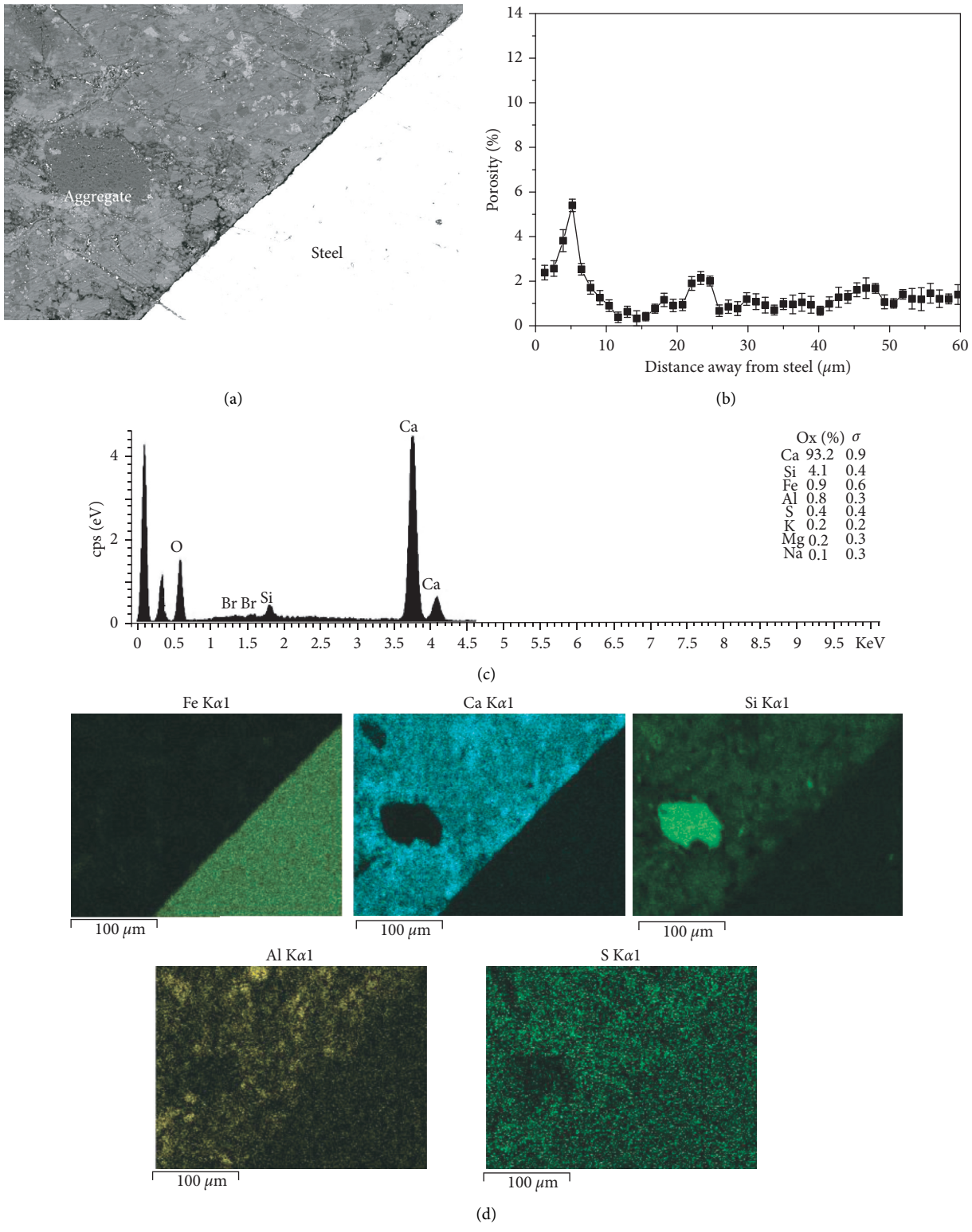

FIGURE 5: Microstructure of steel reinforced OPC concrete aged for 28 d: (a) microstructure of steel reinforced OPC concrete, (b) porosity at steel/concrete interface, (c) EDXA spot analysis of Point '2' at ITZ, and (d) element mappings of Fe, Ca, Si, Al, and S.

agreement with previous research [9] indicating that higher corrosion rates can be observed in the presence of increased voids at ITZ.

EDX spot analysis on Point '2' (Figure 5(c)) illustrates that there is an abundant calcium on reinforcement surface, accounting for as much as 93.2 wt. %. Elemental mapping of

calcium (Figure 5(d)) shows that there exists a discontinuous calcium-enriched layer at the ITZ, which is indicative of the presence of CH and/or C-S-H according to the hydration mechanism of OPC cement. Small amounts of Al can also be found occasionally in the vicinity of steel surface, suggesting the inclusions of ettringite or monosulfate at ITZ. According to the EDX mapping, there is not much Si at the ITZ, which indicates that C-S-H is not abundant at ITZ and is primarily associated with CH. This is consistent with the previous reports that suggested a noncontiguous CH precipitation layer near the steel surface [10].

These results suggest that the interface in steel reinforced OPC concrete is dominated by CH, with some inclusions of ettringite and/or monosulfate phases. However, increased levels of porosity can be observed near the steel surface, which may cause a higher possibility of ion transport in the vicinity of reinforcement, particularly Cl^- and O^{2-}, which may consequently lead to reinforcement corrosion initiation.

4. Conclusions

According to the thermal analysis and XRD results, ettringite is the main hydration product in CSA cement at early stage. With increasing curing ages, strätlingite and monosulfate become dominant in the hydrated CSA cement systems. Polarization potential shows that the steel embedded in CSA concrete remains passive for 28 d in absence of Cl^- ions and carbonation.

Microstructural analysis demonstrates that there is an aluminate-enriched layer at steel/concrete ITZ in steel reinforced CSA concrete, which confirms the wall effect of reinforcement. The main hydration product of this Al-enriched layer is AH_3, which is also alkaline and is expected to improve the steel passivity in absence of Cl^-ions and carbonation. In addition, microstructural observation shows that the steel/concrete ITZ of steel reinforced CSA concrete is of high quality with reduced porosity, which may lead to reduced possibility of current flow between anode and cathode and therefore could improve the corrosion resistance of the embedded reinforcement to some extent.

Data Availability

The data used to support the findings of this study are available from the corresponding author upon request.

Conflicts of Interest

The authors declare that they have no conflicts of interest.

Acknowledgments

This work was supported by the National Natural Science Foundation of China (No. 51674199) and State Key Laboratories of Silicate Materials for Architectures, Wuhan University of Technology in China (No. SYSJJ2019-17).

References

[1] P. Chaunsali and P. Mondal, "Hydration and early-age expansion of calcium sulfoaluminate cement-based binders: experiments and thermodynamic modeling," *Journal of Sustainable Cement-Based Materials*, vol. 5, no. 4, pp. 259–267, 2016.

[2] I. A. Chen and M. C. G. Juenger, "Synthesis and hydration of calcium sulfoaluminate-belite cements with varied phase compositions," *Journal of Materials Science*, vol. 46, no. 8, pp. 2568–2577, 2011.

[3] K. Quillin, "Performance of belite-sulfoaluminate cements," *Cement and Concrete Research*, vol. 31, no. 9, pp. 1341–1349, 2001.

[4] M. C. Martín-Sedeño, A. J. M. Cuberos, Á. G. De la Torre et al., "Aluminum-rich belite sulfoaluminate cements: clinkering and early age hydration," *Cement and Concrete Research*, vol. 40, no. 3, pp. 359–369, 2010.

[5] D. Kalogridis, G. C. Kostogloudis, C. Ftikos, and C. Malami, "A quantitative study of the influence of non-expansive sulfoaluminate cement on the corrosion of steel reinforcement," *Cement and Concrete Research*, vol. 30, no. 11, pp. 1731–1740, 2000.

[6] F. P. Glasser and L. Zhang, "High-performance cement matrices based on calcium sulfoaluminate-belite compositions," *Cement and Concrete Research*, vol. 31, no. 12, pp. 1881–1886, 2001.

[7] M. Carsana, F. Canonico, and L. Bertolini, "Corrosion resistance of steel embedded in sulfoaluminate-based binders," *Cement and Concrete Composites*, vol. 88, no. 1, pp. 211–219, 2018.

[8] C. L. Page, "Mechanism of corrosion protection in reinforced concrete marine structures," *Nature*, vol. 258, no. 5535, pp. 514-515, 1975.

[9] A. Michel, A. O. S. Solgaard, B. J. Pease, M. R. Geiker, H. Stang, and J. F. Olesen, "Experimental investigation of the relation between damage at the concrete-steel interface and initiation of reinforcement corrosion in plain and fibre reinforced concrete," *Corrosion Science*, vol. 77, no. 6, pp. 308–321, 2013.

[10] A. T. Horne, I. G. Richardson, and R. M. D. Brydson, "Quantitative analysis of the microstructure of interfaces in steel reinforced concrete," *Cement and Concrete Research*, vol. 37, no. 12, pp. 1613–1623, 2007.

[11] C. L. Page, "Initiation of chloride-induced corrosion of steel in concrete: role of the interfacial zone," *Materials and Corrosion*, vol. 60, no. 8, pp. 586–592, 2015.

[12] K. V. Subramaniam and M. Bi, "Investigation of the local response of the steel–concrete interface for corrosion measurement," *Corrosion Science*, vol. 51, no. 9, pp. 1976–1984, 2009.

[13] U. M. Angst, M. R. Geiker, and A. Michel, "The steel–concrete interface," *Materials and Structures*, vol. 50, no. 2, p. 143, 2017.

[14] V. G. Papadakis and S. Demis, "Predictive modeling of concrete compressive strength based on cement strength class," *Computers and Concrete*, vol. 11, no. 6, pp. 587–602, 2013.

[15] D. Snoeck, L. F. Velasco, A. Mignon et al., "The influence of different drying techniques on the water sorption properties of cement-based materials," *Cement and Concrete Research*, vol. 64, pp. 54–62, 2014.

[16] M. Song, *Reinforcement Interfaces in Low-Carbon Concretes*, University of Leeds, Leeds, England, 2015.

[17] R. Trauchessec, J.-M. Mechling, A. Lecomte, A. Roux, and B. Le Rolland, "Hydration of ordinary Portland cement and calcium sulfoaluminate cement blends," *Cement and Concrete Composites*, vol. 56, pp. 106–114, 2015.

[18] F. Winnefeld and B. Lothenbach, "Hydration of calcium sulfoaluminate cements - experimental findings and thermodynamic modelling," *Cement and Concrete Research*, vol. 40, no. 8, pp. 1239–1247, 2010.

[19] Y. X. Li, Y. M. Chen, H. T. Zhang et al., "Microstructure and composition of hydration products of ordinary Portland cement with ground steel-making slag," *Journal of Wuhan University of Technology*, vol. 18, no. 4, pp. 76–79, 2003.